

MITS: A Quantum Sorcerer’s Stone For Designing Surface Codes

Avimita Chatterjee

amc8313@psu.edu

Pennsylvania State University

State College, PA, USA

Debarshi Kundu

Pennsylvania State University

State College, PA, USA

dqk5620@psu.edu

Swaroop Ghosh

Pennsylvania State University

State College, PA, USA

szg212@psu.edu

ABSTRACT

In the evolving landscape of quantum computing, determining the most efficient parameters for Quantum Error Correction (QEC) is paramount. Various quantum computers possess varied types and amounts of physical noise. Traditionally, simulators operate in a forward paradigm, taking parameters such as distance, rounds, and physical error to output a logical error rate. However, usage of maximum distance and rounds of the surface code might waste resources. To bridge this gap, we present MITS, a tool designed to reverse-engineer the well-known simulator STIM for designing QEC codes. By curating a comprehensive dataset from STIM using valid physical errors, MITS is equipped to ascertain the optimal surface code parameters for a given quantum computer’s noise model. MITS accepts the specific noise model of a quantum computer and a target logical error rate as input and outputs the optimal surface code rounds and code distances. This guarantees minimal qubit and gate usage, harmonizing the desired logical error rate with the existing hardware limitations on qubit numbers and gate fidelity. We explored and compared multiple heuristics and machine learning models for this task and concluded that XGBoost and Random Forest regression to be most effective, with Pearson correlation coefficients of 0.98 and 0.96 respectively. MITS employs these models to reliably and swiftly achieve the target error rates.

CCS CONCEPTS

- Computer systems organization → Quantum computing; Neural networks.

KEYWORDS

Quantum error correction codes, surface codes, rounds, distance, physical error rate, logical error rate, threshold

1 INTRODUCTION

Quantum Error Correction (QEC) is an indispensable pillar in the advancement of quantum computing. In the quantum realm, where information resides in fragile quantum states, even trivial interactions with the external environment can introduce errors, thereby threatening computational integrity [5, 18]. Quantum systems are uniquely susceptible to two main types of errors: bit-flip and phase-flip. While classical systems often contend with bit-flip errors, the quantum realm introduces the added challenge of phase-flip errors. Classical error correction schemes [2, 12] are ineffective for quantum information due to multiple reasons [21, 22], necessitating QEC. Repetition codes [8], traditional tools in error correction, primarily handle bit-flip errors, making them insufficient for quantum applications. This limitation underscores the importance of surface codes [7]. Surface codes address both bit and phase errors by using a two-dimensional qubit layout. Such an approach makes them a

frontrunner for near-term fault-tolerant quantum computing [19]. Within this category, there are ‘rotated’ [20] and ‘unrotated’ [9] variants. Rotated surface codes offer a higher resistance to errors and are somewhat less complex to implement than the unrotated versions [3]. The need for QEC becomes increasingly crucial as we aim for larger, more reliable quantum systems. It is the key to ensure that the quantum computations are both accurate and consistent.

1.1 Motivation

Quantum computing has made significant strides, prompting an important question: Does enlarging error-correcting codes always result in fewer logical errors in real-world devices? As an illustrative example, consider running a distance 25 rotated surface code of 75 rounds. While this might approach close to fault tolerance, it demands a staggering ~ 580 qubits and utilizes ~ 2040 gates [3]. But is such an extensive setup even necessary? Theory suggests that larger code distances should indeed yield fewer logical errors. Yet, with QEC, while we can substantially lower error rates, this advantage does not come without costs, namely the need for more qubits and longer computation times [1]. Longer computational times may also lead to potential decoherence risks [15]. The effectiveness of QECCs varies based on the specific environmental noise they counteract. Therefore, the right choice of QECC is not solely about minimizing errors; it also entails customizing the code for the quantum computer at hand, specifically their physical error characteristics. Our challenge is identifying the most efficient blend of distance and rounds needed to meet a target logical error rate, given our knowledge of the quantum system’s physical errors.

1.2 Contribution

To the best of our knowledge, MITS is the first tool specifically tailored to account for the physical noise characteristics of quantum systems, to recommend a customized combination of distance and rounds for rotated surface codes. The aim is to achieve a target logical error rate while maintaining an optimal balance between qubit, gate, and time usage. The contributions to building MITS are as follows: ① *Utilization of Quantum Simulation*: We employ STIM [11], a leading simulator for quantum stabilizer circuits. As indicated by a recent study [17], STIM effectively mirrors the performance of QECCs on real quantum machines. Given the qubit limitations in quantum computers, making execution of full QECCs infeasible, STIM proves invaluable for our purposes. ② *Development of MITS from STIM’s Framework*: While STIM operates conventionally – using parameters like distance, rounds, and physical error to yield logical error rates – MITS adopts an inverse approach. We have tailored a dataset from STIM, aiming to infer the optimal distance and round configurations. This reverse engineering substantially

expedites the process, cutting down simulation time. **3 Model Selection using Heuristics and Machine Learning:** Recognizing that one-size-fits-all models are rarely effective, we explored multiple heuristics and machine learning models. This iterative approach allowed us to evaluate and select the best-fit model for our predictive needs, thereby ensuring that MITS's recommendations are reliable. We assume readers are familiar with basic QEC concepts, including classical error correction, repetition codes, stabilizer & encoding circuits, and surface codes. For such background information, one can refer to recent literature on the topic such as [4].

1.3 Structuring the Paper

Section 2 provides a comprehensive overview of surface codes. Section 3 delves into the construction of MITS by ingeniously reverse engineering STIM, dataset creation and the myriad of heuristics and machine learning models considered for the task. In Section 4, we compare the models and further evaluate the chosen model, affirming its robust performance and applicability. Finally, the paper concludes with Section 5.

2 BACKGROUND ON SURFACE CODES

This section provides a detailed examination of the working of surface codes, focusing particularly on the rotated variants and the intricate balance between code distances and rounds.

2.1 Dynamics of Rotated Surface Codes

Before we dive into the workings of rotated surface codes, we must understand the foundations of stabilizers. At the heart of most QECCs lie two key stabilizers: the X-stabilizer and the Z-stabilizer. The role of X-stabilizers is to detect Z-flip or phase-flip errors, while Z-stabilizers identify X-flip or bit-flip errors. As illustrated in Fig. 1 ④, Z-stabilizers, when applied to four data qubits (q_0, q_1, q_2, q_3), produce the syndrome $Z(q_0) \otimes Z(q_1) \otimes Z(q_2) \otimes Z(q_3)$. This syndrome is then projected onto an ancilla qubit, depicted as a yellow-blob. The resulting syndrome measurement, S_z , provides an indication of ± 1 based on the presence of a bit-flip error in the data qubits. In a parallel fashion, X-stabilizers, as shown in Fig. 1 ⑤, interacting with the same set of data qubits, project the syndrome $X(q_0) \otimes X(q_1) \otimes X(q_2) \otimes X(q_3)$ onto the ancilla qubits, marked as a blue-blob. Here, the syndrome measurement, S_x , reveals whether there is a phase-flip error, with outcomes also manifesting as ± 1 .

The surface code operates on an $n \times n$ lattice foundation for an n -distance code, with the vertices in the lattice representing a data qubit. The lattice's design ensures that every qubit is under the surveillance of both X and Z stabilizers, with the mandate to detect phase and bit-flip errors. The presence of an error can alter the outcome of the associated stabilizer checks, indicating its occurrence. As depicted in Fig. 1 ⑥, a distance 5 rotated surface code is illustrated as a 5×5 lattice. Within this configuration, the grey-blobs denote data qubits. Each yellow surface signifies a Z-stabilizer, while the blue surfaces correspond to X-stabilizers. Utilizing a decoding algorithm, the location and nature of these errors can be pinpointed [13, 16]. Once identified, quantum gates intervene to rectify these errors, restoring the affected qubits to their rightful states. The strength of the surface code is its capability

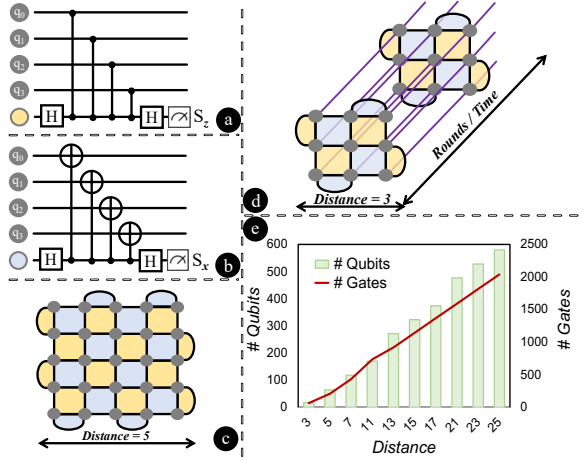


Figure 1: Rotated surface codes: interactions, structures, and overheads. ④ Z-stabilizers interacting with four data qubits (q_0, q_1, q_2, q_3) projects the syndrome, S_z , onto a yellow-blob ancilla. ⑤ X-stabilizers, using the same qubits, generate a corresponding syndrome, S_x , projected onto a blue-blob ancilla. ⑥ A distance 5 rotated surface code forms a 5×5 lattice, with grey-blobs as data qubits and yellow/blue surfaces representing Z/X-stabilizers. ⑦ A distance 3 code across 2 rounds highlights the 3×3 lattice's repetition over time. ⑧ Increased distances raise qubit counts, and more rounds lead to greater gate numbers. With rounds being threefold the distance, the overhead of high distance and rounds is evident.

to amend multiple errors and its robustness amidst noise, as long as the noise level remains below a certain threshold.

The physical error rate reflects errors during individual qubit operations in a quantum computer, while the logical error rate gauges residual errors after applying QECC. The aim of QECCs is to minimize the logical error rate despite high physical errors. The 'threshold' error rate represents the maximum physical error rate a QECC can handle while still reducing the logical error. Beyond this, the QECC becomes ineffective. Modern quantum processors manifest error rates close to 10^{-3} [10, 14]. Intriguingly, surface codes can tolerate an error threshold of approximately 10^{-2} [3, 17], a value that is an order of magnitude higher than what current quantum processors can achieve without error correction.

2.2 Interplay Between Code Distance and Rounds

The distance of a surface code refers to the dimensions of the underlying lattice, with a distance d corresponding to a $d \times d$ lattice. The round pertains to the number of times this lattice pattern is employed in the error correction process. With each round, the code attempts to identify and rectify errors, enhancing the probability of successful error correction, especially in the presence of persistent or recurrent errors. Essentially, for a distance d surface code, the $d \times d$ lattice configuration is iterated for r rounds. In Fig. 1 ⑦, a distance 3 \times 3 rotated surface code is visualized across 2 rounds, demonstrating how the 3×3 lattice pattern is repeated over time. The iteration over multiple rounds signifies the prolonged

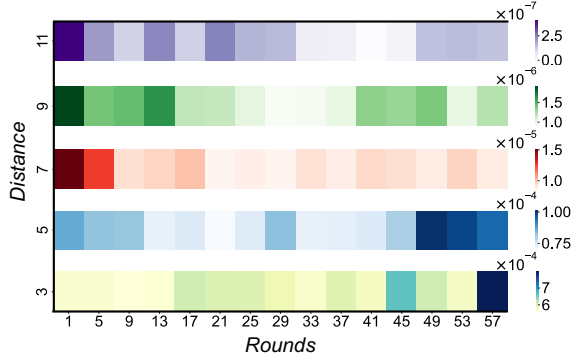


Figure 2: Logical error rate heat map analysis. With increasing distance, the logical error rate shows an anticipated reduction. Yet, there is a nuanced relationship with rounds: the error rate fluctuates initially, reaches a ‘sweet spot’ where distance seems to counterbalance the errors from rounds sufficiently, and subsequently increases again, potentially from heat relaxation risks.

computational duration. It is evident that as the distance escalates, the total data qubits in the system also grow. Likewise, the gate count grows with an augmentation in the number of rounds. This relationship between distance and the increasing tally of qubits and gates is illustrated in Fig. 1 (e). For each distance value considered, the number of rounds is set as three times the distance. The depiction underscores the overhead associated with employing surface codes of increased distance and rounds.

Balancing distance and rounds in surface codes is pivotal to their efficacy. While it might seem tempting, from a theoretical standpoint, to lean towards a minimal distance surface code and ramp up the rounds, this approach encounters practical limitations. First, when the distance of a surface code is extended, there is an inherent need to also boost the rounds. The reason is that increased rounds add more gates, inadvertently introducing more errors. The expanded distance serves as a buffer, offering redundant checks to mitigate and rectify these errors. Secondly, the higher number of rounds inadvertently increases computational time. As a result, the data qubits are more susceptible to heat relaxation & decoherence, introducing additional errors. Hence, the crux lies in meticulously calibrating the equilibrium between distance and rounds, ensuring optimal performance of the code.

In an experiment, we varied the distance and rounds of rotated surface codes and observed the resulting logical error rate (Fig. 2). As expected, an increased distance led to a reduced logical error rate. However, the interplay with rounds was intricate: the logical error rate fluctuated initially until it stabilized, suggesting the distance adequately counteracted the errors introduced by the rounds. This ‘sweet spot’ state persisted for a few rounds before the logical error rate began rising again, likely due to the risk of heat relaxation & decoherence. With a constant physical noise level, the challenge is pinpointing the perfect equilibrium between distance and the corresponding number of rounds to minimize qubit and gate usage.

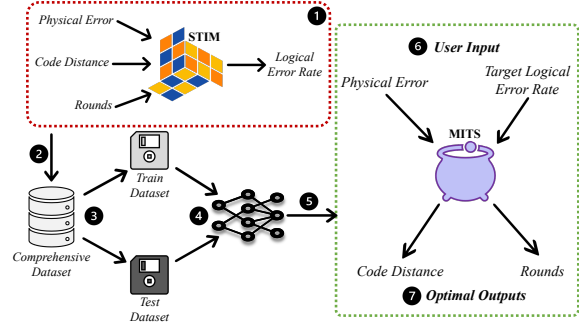


Figure 3: The developmental and operational blueprint of MITS. ① **STIM Simulation:** Using STIM to estimate logical error rates from physical attributes, distance, and rounds. ② **Data Compilation:** Generated a dataset from 8.5k STIM experiments over weeks. ③ **Dataset Partition:** Split into training and test subsets. ④ **Model Exploration:** Evaluated various heuristic and ML models for optimal surface code parameters. ⑤ **Optimal Model Selection:** Chose a two-step model using xgboost and random forest. ⑥ **User Input:** Users specify physical error attributes and desired logical error rate. ⑦ **MITS Output:** MITS recommends optimal distance and rounds.

3 MITS: AN INVERTED APPROACH

3.1 Pivotal Idea

If a user knows the noise level of their quantum machine (typically available for hardware) and has a target error rate in mind, they can input this information into MITS. In return, MITS will recommend the optimal ‘distance’ and ‘rounds’ for a rotated surface code. It will save hours the users would otherwise spend on simulations to refine distance and round using trial-and-error. We prepared a detailed dataset using STIM simulations and then employed various machine learning models and heuristics to predict the distance and rounds. This section first explains the dataset creation followed by testing and selection of the best model. Fig. 3 illustrates the systematic progression of MITS, detailing both its development stages and operational workflow.

3.2 Dataset Compilation from STIM

Utilizing STIM [11], a stabilizer simulator, we estimated logical error rates based on physical error attributes, distance, and rounds of rotated surface codes. In total, we conducted 8640 experiments, culminating in a database built over weeks. Our exploration focused on four types of physical error rates: depolarizing, gate, reset, and readout errors. We determined the error range for each type by examining the minimum and maximum errors across all available IBM quantum computers. This range is representative of most quantum computers and is subject to minimal variation due to calibration. The experiments systematically spanned distances of 3 to 19 and rounds between 1 to 60. Notably, when the logical error rate reached or fell below 10^{-9} in our tests, STIM deems it fault-tolerant. Consequently, any subsequent trials with the current set of error attributes were terminated, preventing redundant additions to the dataset due to

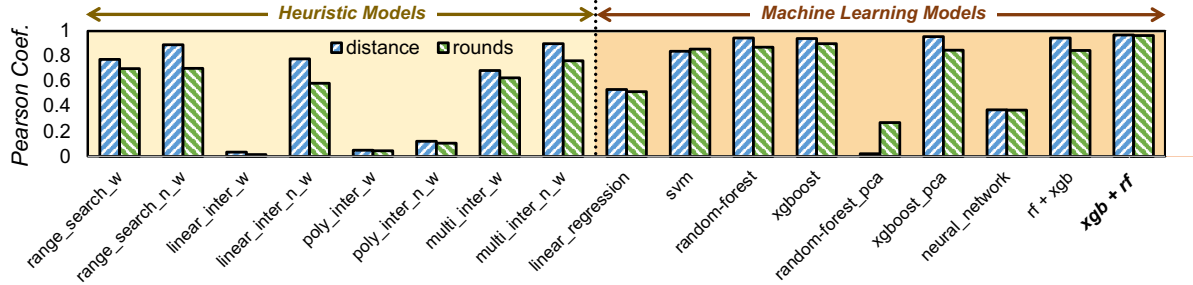


Figure 4: Performance Analysis: Pearson Correlation of Heuristic vs. ML Models. The bar graph compares heuristic (first half) and machine learning (second half) models. The non-weighted multivariate interpolation leads among heuristics but is surpassed by XGBoost and Random Forest in ML. Optimal choices are XGBoost for distance and Random Forest for rounds, highlighted in bold.

the known inverse relationship between error rates and code distance. Drawing from actual quantum computer error levels and carefully curated to exclude redundant values, this dataset stands as the most comprehensive resource tailored for this specific purpose. Across all experiments, we employed the Minimum Weight Perfect Matching (MWPM) decoder [13]. For computational efficiency, the simulations utilized 4 parallel workers, enabling faster execution across multiple CPU cores. The maximum number of trials, or ‘shots’, was set to 1,000,000, with each shot representing a single instance of the quantum error correction process. Post-data collection, we segregated the data, randomly reserving 20% as a test set. Both datasets were pivotal for developing the predictive models that underpin MITS.

3.3 Exploration for Predictive Models

We started with heuristics, as they provide intuitive approaches, before delving into the complexities of machine learning to find the ideal model. We follow a two-step predictive method across all of our models: firstly predicting the code distance using the physical error rate and target logical error rate, and secondly predicting the rounds based on the deduced distance and target logical error rate. This approach is adopted for several reasons. The distance directly influences the logical error rate and serves as a foundational parameter of a surface code. By predicting the distance based on physical error rates and the desired logical error rate, we streamline the process, allowing for a more focused prediction. With the distance determined, the complexity of predicting rounds is reduced. If we aimed to predict both distance and rounds simultaneously, the inherent complexity would rise, potentially compromising the accuracy of our models. It is worth noting that when distance predictions are decimal, we round them up for better round predictions in the subsequent model. The Pearson correlation coefficient [6] measures the correlation between actual and predicted variables; a value near 0 indicates little to no correlation, while a value near 1 suggests a strong positive correlation. Fig. 4 showcases a comparison of all models evaluated during our exploration, using the Pearson coefficient as the metric.

3.3.1 Heuristic Methods. We explored heuristics from two distinct angles. First, we introduced a weight factor for each physical error attribute, reflecting its impact on the entire quantum system. Since

gate errors have the most pervasive effect throughout the system, they are assigned the highest weight. Following this, depolarizing errors are weighted, with readout and reset errors receiving the lowest weights due to their non-propagative nature. On one hand, these aggregated weights serve as the sole feature representing physical error rates in models denoted as ‘weighted (_w)’, eliminating the need to use each of the four attributes independently. On the other hand, in the ‘non-weighted (_n_w)’ models, no specific weights are assigned. Instead, each physical error attribute is considered separately in the prediction process. ① *Search by Range*: This model uses a distance-based heuristic to find the nearest points in a training dataset. It calculates the Euclidean distance between prediction data and training entries, and then retrieves the associated code distance and rounds. ② *Linear Interpolation*: This model performs linear interpolation on a training dataset to estimate distance and round values for a prediction dataset. Linear interpolation is a method of estimating values between two known data points using the formula: $y = y_1 + (x - x_1) \times \frac{y_2 - y_1}{x_2 - x_1}$. The function sorts the training data based on proximity to each reference value from the prediction set and then uses the two nearest points for interpolation. ③ *Polynomial Interpolation*: Using a training dataset, this model fits a 2nd degree polynomial to the three closest points for each prediction value. If the polynomial fit encounters an error, the function gracefully falls back to linear interpolation using the two nearest points. ④ *Multivariate Interpolation*: This function employs multivariate interpolation to estimate distance and round values for a prediction dataset based on a training dataset. For each entry in the prediction set, the function uses the ‘griddata’ method to interpolate values based on the given input attributes. The training data serves as the input points and values for this interpolation.

3.3.2 Machine Learning Models. Our objective was to ascertain whether the machine learning algorithms could offer improved predictive accuracy over the heuristic approaches. ① *Linear Regression*: Using two sequential models, the first predicts a feature distance with hyperparameter tuning via grid search. The predictions then serve as input features for the second model, which predicts the optimal round. ② *Support Vector Regression*: In a two-stage process, the first SVR model predicts a distance using hyperparameter tuning. Its predictions are then used as inputs for the second model, which predicts another target feature. Both stages use five-fold

Table 1: Pearson Correlation Coefficients of Raw and Rounded Distance and Rounds of MITS

Type	Pearson Corr. Coeff.	
	distance	rounds
Raw Prediction	0.982404	0.964948
Rounded Prediction	0.968062	0.964587

cross-validation for robustness. ③ *Random Forest Regression*: The first model predicts a distance based on several features and undergoes hyperparameter tuning. Its rounded predictions, combined with another feature, are inputs for the second model predicting rounds. A variant incorporating principal component analysis was also explored. ④ *XGBoost Regression*: In this two-stage process, the first model predicts a distance and undergoes hyperparameter tuning. Its rounded predictions are then used by the second model to predict rounds, with both stages using five-fold cross-validation. ⑤ *Neural Network*: A two-stage deep learning approach is employed. The first neural network predicts distance, and its predictions serve as input for the second model predicting rounds. Both models have three-layer architectures and use the Mean Squared Error loss with the Adam optimizer.

4 COMPARISON AND EVALUATION

After assessing various heuristics and machine learning models, multivariate interpolation stood out as the top heuristic. Both XGBoost and Random Forest showed similar high performance, as depicted in Fig. 4. We chose one model for distance prediction and another for round prediction, capitalizing on their strengths. While other models could be viable for prediction, the exceptional performance of our chosen models negated the need to explore additional options. This section delves into the details of XGBoost and Random Forest’s roles in distance and round predictions.

Predictive models, in their essence, do not always yield whole number outcomes. For distance, we round up the raw prediction to the subsequent odd number. While theoretically, surface codes can accommodate even distances, in practical scenarios, odd distances have proven to be more resilient and efficient. This is primarily because odd distances offer a better balance of error correction capability, ensuring the system’s robustness. For rounds, we adjust the raw predictions to the nearest whole number. Regardless of the raw value for distance or rounds, we consistently elevate it to the next odd or whole number. This strategy is imperative to consistently achieve the desired logical error rate. Reducing the distance could jeopardize meeting this target rate. Both raw and adjusted predictions are vital in our analysis. In our approach to finalize the MITS, we employed a two-tiered modeling strategy. Initially, we utilized the XGBoost’s *XGBRegressor* for predicting distance. Key parameters for this model included a *learning_rate* of 0.1, *max_depth* of 6, *min_child_weight* of 5, *gamma* of 0.5, and *n_estimators* set to 200. Following this, the predicted distance values were fed into a Random Forest Regressor to predict rounds. The Random Forest model was configured with a *max_depth* of 20, *min_samples_split* of 10, and *n_estimators* set to 10. The training times for the models were approximately 30 minutes and 7 minutes, respectively. The shorter duration for the latter is due to its use of a smaller dataset

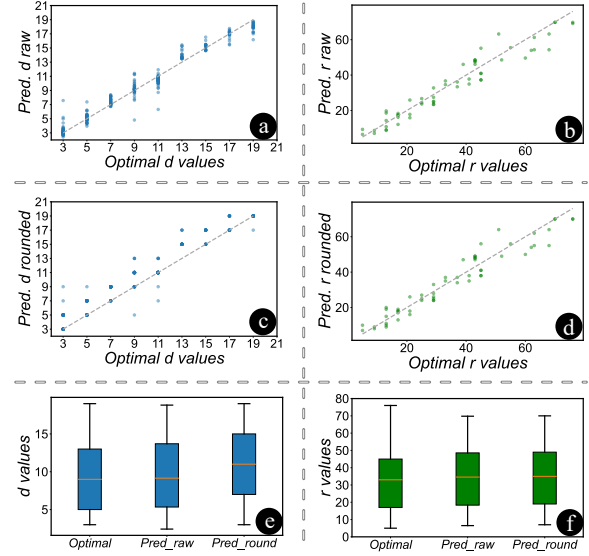


Figure 5: Comparative Analysis of Predicted vs. Optimal Distance and Rounds. ① and ③: Scatter plots comparing predicted and optimal distances, showing a trend towards rounding to the nearest odd number starting at three. ② and ④: Scatter plots of rounds, with raw values generally rounding up to the nearest integer, showing minimal variance. Dotted diagonals indicate perfect predictions. ⑤ and ⑥: Box plots contrasting original, predicted, and rounded values. Distances show deviations upon rounding, while rounds remain consistent across all measures.

containing only distance and target logical error rate attributes, compared to the former which utilized the full dataset. Table 1 displays the Pearson correlation coefficients of these models with respect to raw and rounded values. Hyperparameter tuning with *GridSearchCV* was utilized to prevent overfitting. *Validation on the training dataset yielded correlation coefficients of 0.986 and 0.967 for models predicting d and r, closely matching Pearson coefficients from the test dataset predictions. This similarity confirms the absence of overfitting.*

The scatter plots in Fig. 5 ① and ③ compare the predicted distance values, both in their raw form and when rounded, to the optimal distance values. It is evident from the plots that all distance values are rounded up to the nearest odd number, with a minimum value set at three. In Fig. 5 ② and ④, scatter plots are depicted comparing rounds in their raw form and when rounded. Given that raw rounds are simply rounded up to the nearest integer, there is minimal discernible difference between the two plots. The intricacies and variations among the original, predicted, and rounded values for both distance and rounds can be more comprehensively understood through the box plots. Fig. 5 ⑤ and ⑥ provide a clear visual representation of these values. Upon examination of the data, it is evident that the original and predicted values for distance are closely aligned. However, a noticeable divergence emerges when the predicted values are rounded up to the nearest odd integer. Conversely, for the rounds, there is no discernible difference between the original, predicted, and rounded values. The Pearson correlation coefficients in Table 1 demonstrate that, despite rounding both the

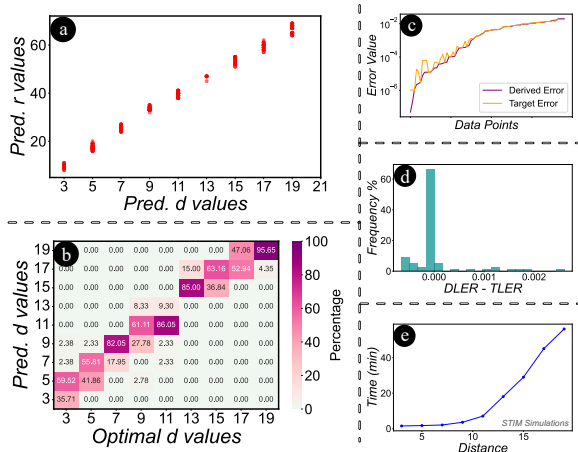


Figure 6: Analysis of Predictions, Error Rates, & Simulation Efficiency. ①: Scatter plot showcasing the correlation between predicted distance and rounds, underscoring the effective prediction in surface codes context. ②: Heatmap of predicted vs. optimal d values. ③: Relationship between derived and target error. ④: Histogram highlighting MITS’s accuracy with a centered distribution at 0 for the difference between DLER and TLER. MITS trends towards reducing logical error rate with minimal negative deviations. ⑤: STIM simulation time growth with increasing d and r, underscoring MITS’s efficiency in reducing time to around 11 ± 3 milliseconds.

distances and rounds, the predicted results remain closely aligned with the actual values.

Next, we evaluate the logical error rates. To begin with a recap, it is essential to note that for surface codes to yield optimal results, there is a necessity to increase the rounds in tandem with the distance. Fig. 6 ① illustrates a scatter plot comparing the predicted distance and rounds. The evident trend of increasing rounds with the rise in distance underscores our assertion. In Fig. 6 ②, we present a heatmap illustrating the comparison between predicted d values and their optimal counterparts. This visualization aids in determining the frequency with which certain values are predicted as d. Particularly, we focus on instances where predictions fall below the optimal values, as these cases signify potential failures to achieve the target logical error rate. We performed another experiment to validate the logical error rate obtained from STIM by using the d and r values predicted by MITS and comparing them against the target logical error rate. In Fig. 6 ③, the relationship between the derived error and the target rate is illustrated. Notably, the derived error rate is predominantly lower than the target rate, with a few exceptions exhibiting minimal discrepancies. We quantify the discrepancy between the Derived Logical Error Rate (DLER) and the Target Logical Error Rate (TLER) by subtracting them. Fig. 6 ④ presents a histogram illustrating the frequency distribution of this difference. From the histogram, it is evident that the predominant distribution is centered at 0, affirming that MITS consistently achieves the target logical error rate. A significant portion of the distribution also leans towards the positive side, indicating that MITS often surpasses the target by reducing the logical error rate even further – a favorable outcome. There is a minor distribution

on the negative spectrum, the magnitude of these differences is so minuscule that they can be considered negligible. Figure 6 ⑤ depicts the exponential increase in STIM’s simulation time for rotated surface codes as distance d and rounds r grow. For our study, rounds are set at almost three times the distance. Given this time increase for just one set of physical errors, iterative trials for the optimal settings could be significantly time-consuming. A user with specific physical errors targets a particular logical error. Starting with the smallest distance d, reaching the target takes 2.736 hours for one round. Adjusting rounds extends this by r times. Even with binary search halving time, it is a long simulation. And if the user has multiple physical error variations and targets? The time demand becomes even more daunting. Consequently, it is evident that MITS significantly reduces simulation time from hours to 11 ± 3 milliseconds on a pre-trained model, swiftly predicting the required distance and rounds to achieve a specified target logical error rate.

5 CONCLUSION

This paper presented MITS, a new methodology to optimize surface code implementations by predicting ideal distance and rounds given target logical error rates and known physical noise levels of the hardware. By devising an inverse modeling approach and training on a comprehensive simulation dataset of over 8500 experiments, MITS can rapidly recommend surface code parameters that balance qubit usage with error rate goals. Our comparative assessment validated the efficacy of the XGBoost and Random Forest models underpinning MITS’s predictions, which achieved Pearson correlation coefficients of 0.98 and 0.96 for distance and rounds respectively. We further confirmed that the predicted combination of distance and rounds from MITS consistently attained the target logical error rates, with deviations centered around 0. MITS can cut hours from surface code calibration, assisting in the realization of practical error-corrected quantum processors.

REFERENCES

- [1] Dorit Aharonov et al. 1997. Fault-tolerant quantum computation with constant error. In *Proceedings of the twenty-ninth annual ACM symposium on Theory of computing*, 176–188.
- [2] David T Brown. 1960. Error detecting and correcting binary codes for arithmetic operations. *IRE Transactions on Electronic Computers* 3 (1960), 333–337.
- [3] Avimita Chatterjee et al. 2023. Demystifying Noise Resilience of Quantum Error Correction: Insights for Code Optimization. *arXiv preprint arXiv:2308.02769* (2023).
- [4] Avimita Chatterjee et al. 2023. Quantum Error Correction For Dummies. *arXiv preprint arXiv:2304.08678* (2023).
- [5] Aashish A Clerk et al. 2010. Introduction to quantum noise, measurement, and amplification. *Reviews of Modern Physics* 82, 2 (2010), 1155.
- [6] Israel Cohen et al. 2009. Pearson correlation coefficient. *Noise reduction in speech processing* (2009), 1–4.
- [7] Eric Dennis et al. 2002. Topological quantum memory. *J. Math. Phys.* 43, 9 (2002), 4452–4505.
- [8] Simon J Devitt et al. 2013. Quantum error correction for beginners. *Reports on Progress in Physics* 76, 7 (2013), 076001.
- [9] Austin G Fowler et al. 2012. Surface codes: Towards practical large-scale quantum computation. *Physical Review A* 86, 3 (2012), 032324.
- [10] Brooks Foxen et al. 2020. Demonstrating a continuous set of two-qubit gates for near-term quantum algorithms. *Physical Review Letters* 125, 12 (2020), 120504.
- [11] Craig Gidney. 2021. Stim: a fast stabilizer circuit simulator. *Quantum* 5 (2021), 497.
- [12] Richard W Hamming. 1950. Error detecting and error correcting codes. *The Bell system technical journal* 29, 2 (1950), 147–160.
- [13] Oscar Higgott. 2022. PyMatching: A Python package for decoding quantum codes with minimum-weight perfect matching. *ACM Transactions on Quantum Computing* 3, 3 (2022), 1–16.

- [14] W Huang et al. 2019. Fidelity benchmarks for two-qubit gates in silicon. *Nature* 569, 7757 (2019), 532–536.
- [15] Julian Kelly et al. 2015. State preservation by repetitive error detection in a superconducting quantum circuit. *Nature* 519, 7541 (2015), 66–69.
- [16] Vladimir Kolmogorov. 2009. Blossom V: a new implementation of a minimum cost perfect matching algorithm. *Mathematical Programming Computation* 1 (2009), 43–67.
- [17] Sebastian Krinner et al. 2022. Realizing repeated quantum error correction in a distance-three surface code. *Nature* 605, 7911 (2022), 669–674.
- [18] G Mouloudakis et al. 2021. Entanglement instability in the interaction of two qubits with a common non-Markovian environment. *Quantum Information Processing* 20 (2021), 1–15.
- [19] Peter W Shor. 1996. Fault-tolerant quantum computation. In *Proceedings of 37th conference on foundations of computer science*. IEEE, 56–65.
- [20] Yu Tomita et al. 2014. Low-distance surface codes under realistic quantum noise. *Physical Review A* 90, 6 (2014), 062320.
- [21] John Von Neumann. 2018. *Mathematical foundations of quantum mechanics: New edition*. Vol. 53. Princeton university press.
- [22] William K Wootters et al. 2009. The no-cloning theorem. *Physics Today* 62, 2 (2009), 76–77.